

Structural and performance radiation protection the phosphate glasses contain: Te, K, Al, Nb-doped with rare earth

M. S. Alqahtani^{a,b,c*}, F. Alqahtani^d, A. M. Almarhaby^e, K. I. Hussain^{a,f},
Y. Khalid^a, H. Almohiy^b, I. S. Yaha^{c,g}, El S. Yousef^{c,d}

^aResearch Center for Advanced Materials Science (RCAMS), King
Khalid University, Postcode: 9004, Zip code: 61413, Abha, Saudi
Arabia

^bRadiological Science Department – Faculty of Applied Medical Science
– King Khalid University, Zip code 61413, P. O. Box 9004, Abha, Saudi
Arabia

^cBioImaging Unit, Space Research Centre, Michael Atiyah Building,
University of Leicester, Leicester, LE1 7RH, U.K.

^dDepartment of Radiological Sciences, College of Applied Medical Sciences,
Najran University, Najran 1988, Saudi Arabia

^eRadiology Department, King Fahd General Hospital, Postcode: 23325,
Jeddah, Kingdom of Saudi Arabia

^fDepartment of Medical Physics and Instrumentation, National Cancer
Institute, University of Gezira, Wad Medani 20, Sudan

^gNanoscience Laboratory for Environmental and Bio-Medical
Applications (NLEBA), Semiconductor Lab., Metallurgical Lab. 2
Physics Department, Faculty of Education, Ain Shams University, Roxy,
Zip Code 11757, Cairo, Egypt

Because of the increased use of ionizing radiation, radiation management and security procedures are now regarded a standard part of many therapeutic and specialist fields. The focus of this work is on the radiation security features of Novel Oxide Glass (PZBKTANer). The unique glass assembly is 40P2O5-30ZnO- 20BaF2-3.8K2TeO3-1.2Al2O3-5Nb2O5-3Er2O3 in mol percent (test code PZBKTANer). For the suggested oxide glass, several radiation shielding characteristics have been investigated for a specific energy range of ionizing radiation. The linear and mass attenuation coefficients, mean free path, half-value layer, total nuclear and electronic cross-sections, and fast neutron expulsion cross-section are among the radiation shielding properties. Furthermore, the unique fabricated glass (PZBKTANer) was compared to commonly used radiation protection compositions, such as RS-253 G18, RS-360, RS-520, Chromite, Ferrite, Magnetite, and Barite glass, as well as RS-253 G18, RS-360, RS-520, Chromite, Ferrite, Magnetite, and Barite glass. Also, we studied the structure of fabrication by using Raman spectra. The findings suggest that the new oxide glass might be used in a broad variety of ionizing radiation applications for protection in both therapeutic and industrial applications.

(Received May 2, 2022; Accepted January 11, 2023)

Keywords: Raman, Structural, Half-value layer, Mean free path,
Cross section of neutron removal, Shielding of radiation

1. Introduction

Glasses have recently been included as a new component for gamma radiation protection. Glass has a number of characteristics, including precise optical clarity, true mechanical properties, heat resistance, and significant attenuation, particularly in heavy metal Oxide samples. Another

* Corresponding author: mosalqhtani@kku.edu.sa
<https://doi.org/10.15251/CL.2023.201.43>

significant factor to consider is the flexibility with which the glass composition may be adjusted to provide acceptable protection [1- 10]. A customized oxide glass with novel features may be constructed to test the shielding against ionizing radiation. It's created from a variety of oxide glasses that have previously undergone radiation testing. Natural sources of ionizing radiation, such as limitless beams and earthborn radioactive sources like thorium and uranium found in rocks and minerals, have an impact on humans all around the world. Individuals are illuminated by human-made sources such as therapeutic and diagnostic radiation sources for medical purposes, such as radiopharmaceuticals, external x-rays, and gamma rays. Indeed, fundamental human-made sources are known as buyer goods, which are used in construction and street development materials, X-ray security devices, and combustible powers such as coal [11- 24]. A broad range of ionizing radiation energy has been investigated and rigorously tested against particular chemical compounds like lead (Pb) [11,12]. Lead is often used to protect against ionizing radiation. It has a limited number of applications. It has a high amount of toxicity, is quite expensive, and has a low softening point [13]. These restrictions have prompted researchers to investigate other materials, such as glass, polymers, ceramics, and concrete, that seem to provide cost-effective, efficient, and effective radiation shielding compositions [14–19].

The optical and shielding properties of such glasses have inspired many researchers to see their utility as a safety replacement device in medical workplaces, X-ray and atomic projects in the field of inventions, X-ray equipment, gamma camera rooms, and computed tomography (CT) examination workplaces [11, 12, 24-29, 31]. The radiation-protecting properties of Erbium Zinc-Tellurite glass were examined by Tijani et al. [30] to compare a wide range of radiation energy utilized in health and medical imaging applications (20 keV, 30 keV, 40 keV and 60 keV). Our research looks at the photon energy-protecting properties of Novel glass (40P₂O₅- 30ZnO- 20BaF₂- 3.8K₂TeO₃- 1.2Al₂O₃- 5Nb₂O₅- 3 Er₂O₃). We fabricated the unique oxide glass to examine its photon energy shielding characteristics, such as the linear attenuation coefficient (LAC), mass attenuation coefficient (MAC), half-value layer (HVL), and atomic and electronic cross-sections, in order to investigate natural processes (ACS and ECS)

2. Methods and Materials

The glass formula contains mol% of 40P₂O₅- 30ZnO- 20BaF₂- 3.8K₂TeO₃- 1.2Al₂O₃- 5Nb₂O₅- 3 Er₂O₃ (sample code PZBKTANEr). The weights of the developed glass and the molar fractions of the components are presented in Table 1. In this study we used the recently developed software Phy-X / PSD to calculate different screening factors for a wide range of ionizing radiation energies [32].

The linear attenuation coefficient calculates the ratio of mono-energetic photons to the penetration depth in the attenuated case. The linear attenuation coefficient is responsible for the relationship of ionizing radiation and matter, such as the photoelectric effect, the Compton scattering and the Rayleigh effect. How the coefficient of linear attenuation (i. Beer-Lambert's law) is exponentially calculated can be seen in the following equation:

$$I = I_0 e^{-\mu t} \quad (1)$$

Here I represent the weakened ionizing radiation and I_0 denotes unattenuated ionizing radiations. The μ signifies a linear attenuation coefficient (cm⁻¹) and t is the predicted density (cm) of the material.

The mass attenuation coefficient (MAC), which determines the capacity of ionizing radiations to enter a particular substance, can be scientifically communicated utilizing the following equation:

$$\mu_m = \frac{\mu}{\rho} \quad (2)$$

where μ_m is the mass attenuation coefficient (MAC) and ρ outlines the material thickness.

The modeled oxide glass used in our study was a complex material containing more than one component. Therefore, for accurate measurement of mass attenuation coefficient value the following equation was utilized:

$$\mu_{\text{m}} = \frac{\mu}{\rho} = \sum_i w_i (\mu/\rho)_i \quad (3)$$

In which w_i is the fractional component i weight

Table 1. Chemical components density and weight fractions of the elements used designed for the PZBK TANEr study.

Sample code	Composition in mol%	Density (g/cm ³)	The fraction of elements by weight in %									
			P	O	Zn	Ba	F	K	Te	Al	Nb	Er
PZBK TANEr	40P ₂ O ₅ - 30ZnO- 20BaF ₂ - 3.8K ₂ TeO ₃ - 1.2Al ₂ O ₃ - 5Nb ₂ O ₅ - 3Er ₂ O ₃	4.26749	0.1631	0.2939	0.1291	0.1808	0.0500	0.0196	0.0319	0.0043	0.0612	0.0661

The collective atomic and electronic cross-sectional values (ACS, ECS) for beams of single energy (e.g., X or gamma rays) describe the potential for ionizing photons to interact with atoms and electrons at the desired radiation intensity. All these characteristics are calculated in units of cm²g⁻¹ Mathematically by the following equations:

$$\text{ACS} = \sigma_{\text{T}} = \frac{\mu}{\rho} = \frac{\sum_i f_i A_i}{N_A} \mu_{\text{m}} \quad (4)$$

$$\text{ECS} = \sigma_{\text{e}} = \left[\frac{1}{N_A} \right] \sum_i \left[\frac{f_i A_i}{Z_i} (\mu_{\text{m}})_i \right] \quad (5)$$

where N_A refers to the Avogadro number, A_i denotes the atomic weight, the atomic number is shown by Z_i , and f_i is the mol segment of the i^{th} element of the composite in the radiation protection substance.

The half-value layer (HVL) is one of the distinguishing features of radiometric applications. It can be defined as the thickness required to harden half the strength of a single energy beam. The mean free path (MFP) can be defined as the mean distance through the radiation exchange sets of an energetic photon moves. We can use the calculated LAC value to derive both variables and describe them mathematically by solving the given equations:

$$\text{HVL} = \frac{\ln 2}{\mu} \quad (6)$$

$$\text{MFP} = \frac{1}{\mu} \quad (7)$$

The obvious effect of atomic number and electronic density on the radiation atomic products with high atomic number and high electron density may be strongly related to the efficiency of the radiation-absorbing material. Different radiation protection products will be considered by effective atomic number (Z_{eff}) and effective electron density (N_{eff}). Z_{eff} and N_{eff} are defined in mathematical terms as given below:

$$Z_{\text{eff}} = \frac{\sigma_{\text{T}}}{\sigma_{\text{e}}} \quad (8)$$

$$N_{\text{eff}} = \frac{N_A}{\sum_i f_i A_i} Z_{\text{eff}} \sum n_i = \frac{\mu_m}{\sigma_e} \quad (9)$$

where the overall number of collective substances describing the expected radiation-protecting constituents is defined by $\sum n_i$.

The equivalent atomic number (Z_{eq}) is a variable that indicates the radiation shielding properties of a prototype shielding material in terms of its equivalent components. Mathematically, Z_{eq} can be interpreted as follows:

$$Z_{\text{eq}} = \frac{Z_1 (\log R_2 - \log R) + Z_2 (\log R - \log R_1)}{(\log R_2 - \log R_1)} \quad (10)$$

Fractions of the mass attenuation coefficient of Compton dispersion to the the mass attenuation coefficients of the shielding materials ($\mu_{\text{comp}}/\mu_{\text{total}}$) are R_1 and R_2 , showing the reference materials' atomic numbers Z_1 and Z_2 .

Collided and non-collided, two types of photons are created by the method of ionizing radiation photons entering a given protecting medium. The exposure build-up factor (EBF) is defined as the ratio between the total number of photons at a given stage to the number of non-colliding photons. The exposure build-up factor values can be obtained using the G-P method used by the American National Standard ANSI / ANS-6.4.3-1991[33]. After acquiring the required variables, the exposure build-up factor can be computed as follows:

$$C = \frac{C_1 (\log Z_2 - \log Z_{\text{eff}}) + C_2 (\log Z_{\text{eff}} - \log Z_1)}{(\log Z_2 - \log Z_1)} \quad (11)$$

The G-P fitting arguments that consistent with the atomic numbers (Z_1 and Z_2) are considered as C_1 and C_2 in the equations.

The exposure build-up factor (EBF) will be measured by using the given below equation:

$$B(E, x) = 1 + \frac{(bC-1)}{(K-1)} (K^x - 1), K \neq 1 \quad (12)$$

$$B(E, x) = 1 + (b - 1)x, K \neq 1 \quad (13)$$

$$B(E, x) = cx^a + d \frac{\tanh\left(\frac{x}{x_k} - 2\right) - \tanh(-2)}{1 - \tanh(-2)}, x \leq 40 \text{ mfp} \quad (14)$$

The distance between the origin of ionizing radiation and the radiation detector is indicated by x in mean free path (MFP) units. E is the energy of the incident photons, (\mathbf{X}_k , \mathbf{b} , \mathbf{a} , and \mathbf{d}) are the related variables for G-P calculations, and $\mathbf{K}(\mathbf{E}, \mathbf{x})$ is the multipliable dose factor.

The fast neutron removal cross-section (FNRCSS) is calculated using the following calculation to neutron activities of various shielding materials

$$\Sigma_R = \sum_i \rho_i (\Sigma_R/\rho)_i \quad (15)$$

where the fractional density is expressed by ρ_i and $(\Sigma_R/\rho)_i$. The mass removal cross-section measurements were chosen from Chilton, A. B. for the components used in this analysis [34]. All measurements were performed using the software Phy-X / PSD [35].

3. Results and Discussion

Employing the Phy-X / PS code, we tested the attenuated coefficient of the prototype radiation protection material (PZBKTER), which used the spectrum of mono-energetic gamma radiations of 0.01-15 MeV. Radiation exposure factor of gamma photons depend on the intensity of the photon, while increasing the intensity of the incoming photon decreased the value of the

linear attenuation coefficient (LAC) as has been reflected in Figure-1A. In addition, when the material was exposed to low photon energy (i.e., 0.015 MeV), high the linear attenuation coefficient (LAC) values at 152 cm^{-1} were noted. A similar behavior was observed in the statistical measure of mass attenuation coefficient (MAC) values; the observed MAC value was $35.7 \text{ cm}^2 / \text{g}$ at 0.015 MeV. (Figure-1 B).

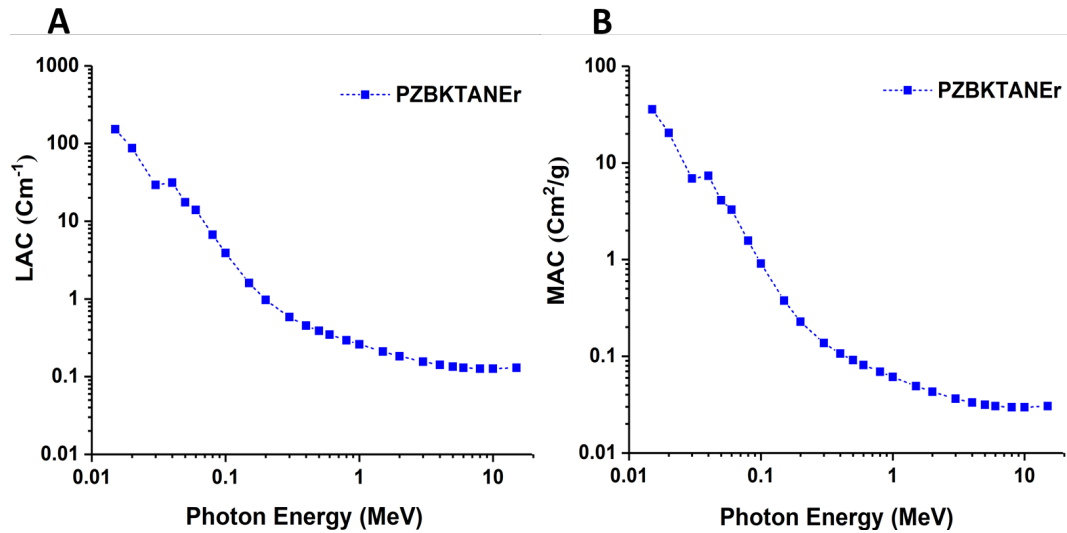


Fig. 1. Graph drawing of the reported measures for the linear (A) and mass attenuation coefficients (B) of the new radiation protection product (PZBKTAner).

For both linear and mass attenuation coefficients, when tested material was exposed to low gamma energy (between 0.015 and 0.04 MeV), there was a dramatic decline in values that could be associated with the presence of photoelectric effect interactions. Exposure to intermediate energy gamma photons (from 0.04 to 3 MeV) lead to a gradual drop-off in linear and mass attenuation coefficients measurements. This activity is attributed to the Compton scattering collision between the incoming photons and the oxide glass material. For gamma-ray energies above 3 MeV, the LAC and MAC values showed a partial reduction because the collision between the incident photons and the oxide glass materials were in the area of pair-production.

The half-value thickness is an important factor of radiation protection and usually provides a clear definition of the thickness of the shielding substance necessary to strengthen half of the strength of the incident ionizing photons. We calculated the half-value thickness values for the 'PZBKTAner' material; these values change as a function of the energies of the incident photon (Figure-2). The interaction of gamma photons with different energies of the novel glass (PZBKTAner) generated lower half-value thickness range than RS-253-G18 shielding glass, whereas other shielding glasses such as RS-360, RS-520, Chromite, Ferrite, Magnetite and Barite have lower values than our novel glass material. For example, the defined half-value thickness values are 0.00455 cm and 5.31871 cm for our novel glass material, while the commercially available shielding glasses RS-253-G18 have 0.02492 cm and 12.11379, RS-360 has half-value thickness values of 0.00245 and 4.23877 cm, RS-520 has 0.00142 and 2.64221 cm at 0.015 and 15 MeV, correspondingly. (Figure-2).

The tested material showed better hardness for incident gamma photons than the commonly available RS-253 G18 safety glass, while other types of shielding glass (such as RS-360 and RS-520 shielding glass) displayed stronger attenuation patterns (Figure-2). This is strong evidence that the values of the acquired half value thickness depend on the density of the irradiated material (Figure 2). Doping the material with a higher atomic number of compounds can be accomplished by increasing the density of various chemical compositions for radiation protection purposes. The effect of density on the values of half value thickness and the photon hardening

process of incident ionizing radiation have been defined in a series of research study results [36 - 38].

Half value thickness (HVL) values given to PZBKtANEr and RS-253 G18 glass at 15 MeV were 5.31871 cm and 12.11379 cm correspondingly, for RS-360 and RS-520, Half value thickness values were 4.23877 cm and 2.64221 cm. Importantly, with minimal variations, the low-photon energy domain (i.e. < 0.2 MeV) was observed. Based on these results, the proposed novel shielding materials would theoretically be used in the medical field for various radiation treatments using low photon energies. For radiation protection purposes, this type of material can be used for a variety of medical imaging methods, including computerized x-ray modalities, and for most of the nuclear medicine procedures involving injection of radioactive gamma emitters, such as Technetium-99 m (Energy = 141 keV).

The average free path (MFP) is an integral function that can be used for radiation shielding to determine a given material and describes the interaction between the photons of the incident radiation and the atoms of the radiation-absorbing material. Stronger protective properties are shown with for the materials showing average free path. As a function of striking photon energy (MeV), Figure 2B shows the calculated average free path values for the proposed PZBKtANr shielding material. In fact, we compared the calculated average free path values for different protective materials. Similar trends to the documented half value thickness values were noticed in the statistical process for the average free path values. Low average free path values were recorded for denser materials, leading a considerable attenuation effect as compared to less dense materials (Figures-2A and 2B).

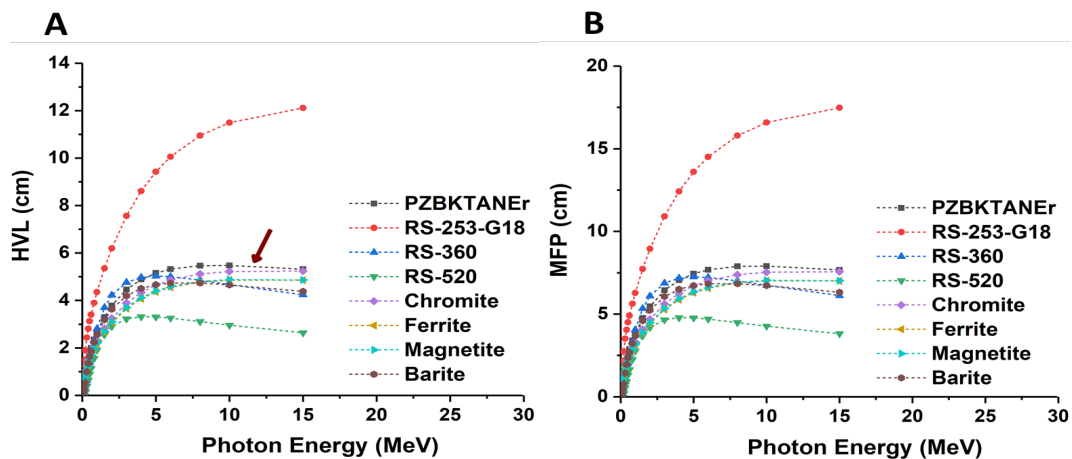


Fig. 2. Graph showing the values for the documented half value thickness (HVL) (A) and average free path (MFP) (B) and comparison of the results for certain radiation-shielding materials to other HVLs and MFPs.

The collective measurements for atomic cross section (ACS) and electronic cross section (ECS) are expressed in figures 3A and 3B. These measurements render a simple possibility of the radiation interaction of every atom or electron in every unit of volume of radiation protection material. A greater number of atoms or electrons in a given unit of volume of matter created a higher documented measurement for ACS and ECS proves that the tested material is more suitable for radiation protection uses. Comparative differences for atomic and electronic cross section measurements are shown graphically in Figures -3A and 3B. The composition of the PZBKtANEr material shows that the both measurements were documented at at 0.015 MeV were 1.88×10^{-21} cm^2/g and 5.15×10^{-23} cm^2/g respectively. The results obtained from these measurements correspond to the functions described earlier as well as the values obtained above. Similarly, we the pattern we found for these measurements as shown in Figures -3A and 3B, Confirmed the same result recorded elsewhere [39].

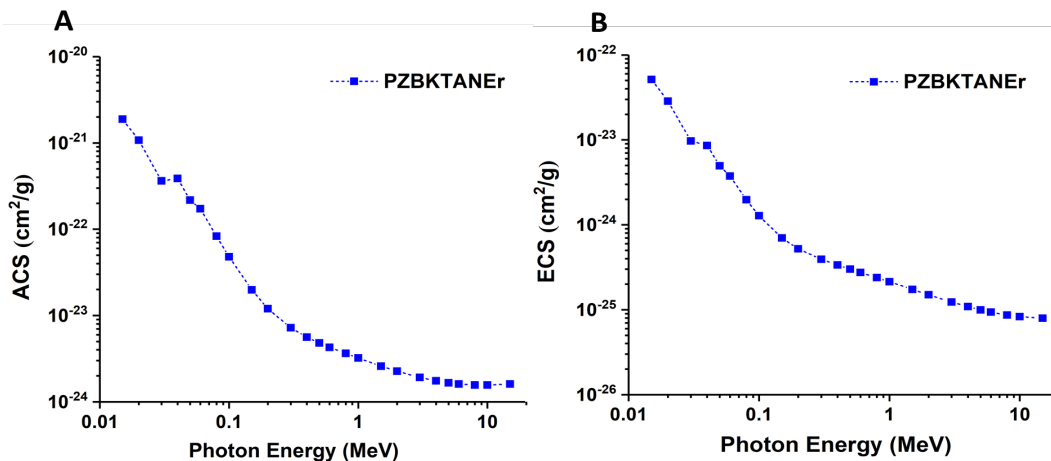


Fig. 3. Line plots displaying the combined measures of atomic cross section (ACS) (A) and electronic cross-sections (ECS) (B).

The atomic and the electron numbers are used to describe the properties of the under-investigation substance. These values are said to be useful by the atomic and the electron numbers (Z_{eff} and N_{eff}) for a material that has more than one constituent components. Knowledge of the energy-dependent measurements for atomic and the electron numbers reveals a complete information of the characteristic of the proposed material against incident ionizing photons when preparing a radiation-protecting substance for gamma-emission applications. Figure-4 shows that the observed measurements for PZBKTANEr in the region of low ionization photon energies (photoelectric effect zone) were higher for Z_{eff} and N_{eff} . These measurements are influenced by the energy of the incoming photon, these measurements dropped significantly in the low-energy range (because of photoelectric effect) and stayed in a fairly constant state in the medium-energy region (Compton scattering) before gradually developing higher values in the high-energy region (pair production). N_{eff} 's value is closely related to ECS and MAC readings. The values obtained were determined on the basis of reported ECS and MAC measurements. The prominent humps at 0.04 MeV for N_{eff} values and 0.06 MeV for Z_{eff} in the curves speculate the regions of K-shell absorption for the (PZBKTANEr) Novel oxide glass.

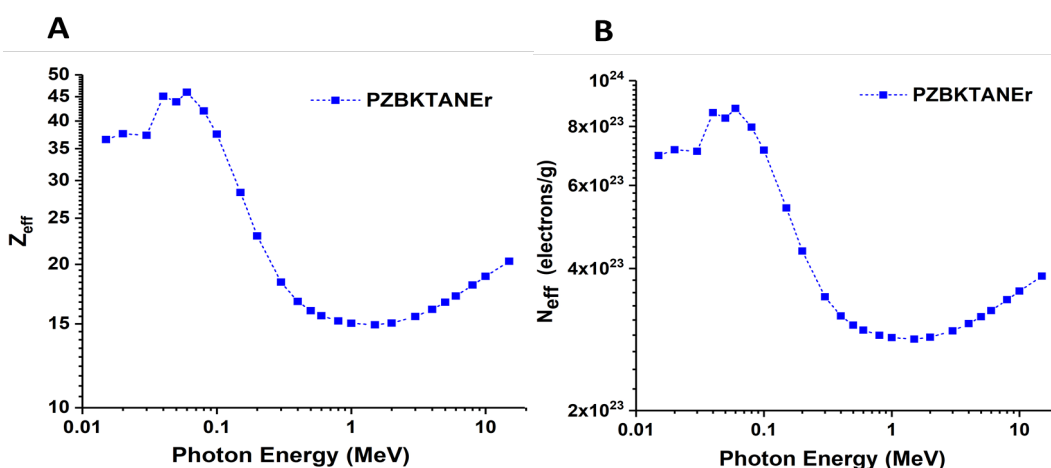


Fig. 4. Graph showing the differences in the effective atomic number (A) and the effective electron density (B) as an energy map of ionizing radiation.

The atomic equivalent number (Z_{eq}) is very significant feature in the calculations of exposure build-up factor (EBF), in terms of an equivalent element, it can be characterized as the radiation protection characteristics of a particular material. In this study, only for the ionization

energy range of 0.015 to 15 MeV, the atomic equivalent number values were measured from the Compton scattering interaction. The maximum recorded value of atomic equivalent number was obtained at 1 MeV. As a result of the Compton scattering process, a gradual increase in Z_{eq} values was observed in the region of medium energies while these values dropped rapidly in the high energy range (> 1 MeV) due to the pair-production effect.

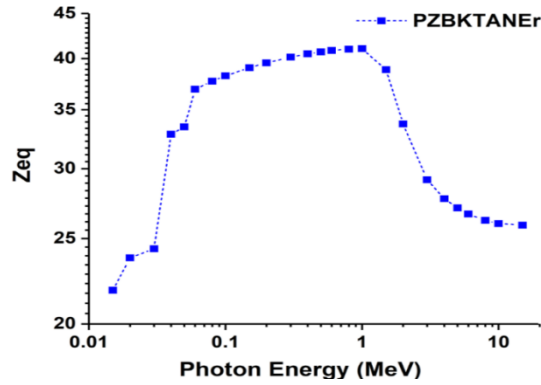


Fig. 5. Depending on the strength of striking ionizing photon, the line plot interprets the difference in the equivalent atomic number (Z_{eq}).

In this research, we evaluated the exposure build-up factor (EBF) and tested it with a different scopes of photon energies, from 0.015 to 15 MeV (Figure-6) and found that the calculated measurements were low in low energy and high energy range, which is the verification pair-production and photoelectric phenomenon. In the photoelectric absorption region (low energy domain), most incident photons are absorbed without extra transfer of energy or secondary interactions. In the middle range of photon energy ($0.04 < E < 3$ MeV), an increase in EBF measurements were noticed due to Compton effect, the incident photons were not fully absorbed by the shielding material. Such activities increase the formation of secondary photons that give rise of interaction in the matter. The incident photons are more active in the high energy environment which result in high penetration and limited interaction with the shielding material. Furthermore, higher EBF values were observed with deeper penetration. Particularly, the use of PZBKATANer novel glass gave rise to high documented values at low incident photon energies (Figure 6 B); sharp increase confirming the fact that the material component is high atomic number metallic element (Erbium, Er, $Z = 68$). The high atomic number factor in the shielding material promotes greater extent of further secondary radiation interactions (MFP).

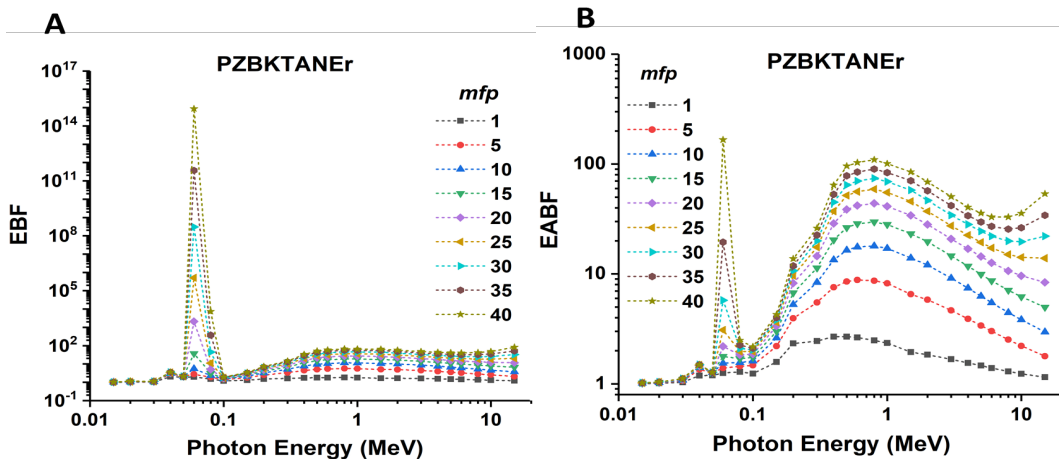


Fig. 6. Line plots display the measurements regarding reported build-up factor of exposure (EBF) and energy absorption (EABF) as a function of electromagnetic radiation, considering the space amongst the cause of ionizing rays and the sensor of rays (MFP).

The particular build-up factor of exposure (EBF) and energy absorption (EABF) and PZBKTA_{Er} Glass photon energy at G-P fitting coefficients (a, b, c, d and X_k) are shown in Figure-7 [40-42]. The upsurge in penetration depth allows the EBF and EABF values to rise due to frequent interactions and photon build-up. This reflects that PZBKTA_{Er} Glass has the maximum Z_{eq} values and minimum measurements of EBF and EABF. The build-up factor of exposure (EBF) and energy absorption (EABF) measurements depend upon the chemical structure and atomic numbers of the substance. Higher radiation protection capabilities are represented by smaller values of EBF and EABF.

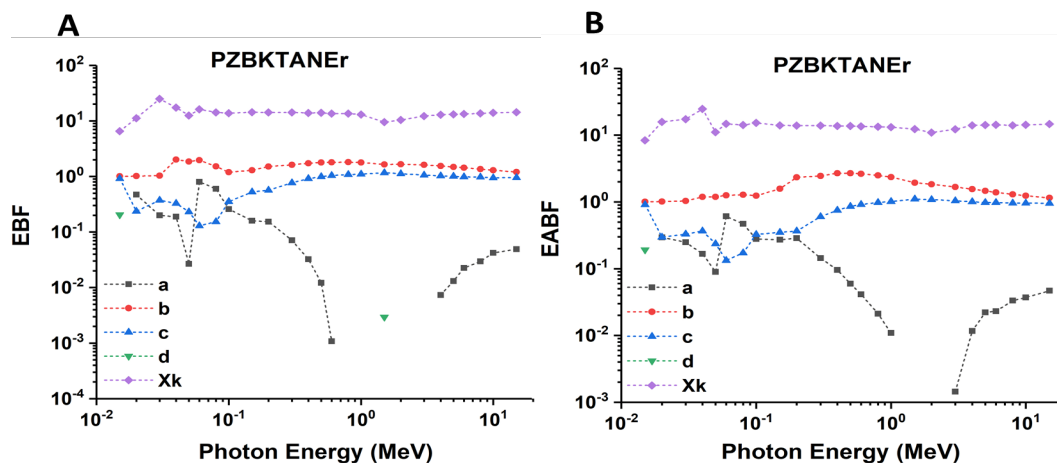


Fig. 7. Graphs representing build-up factor of exposure (EBF) and energy absorption (EABF) and the energy of the photon of the oxide glass (PZBKTA_{Er}) at G-P fitting coefficients (a, b, c, d, and X_k).

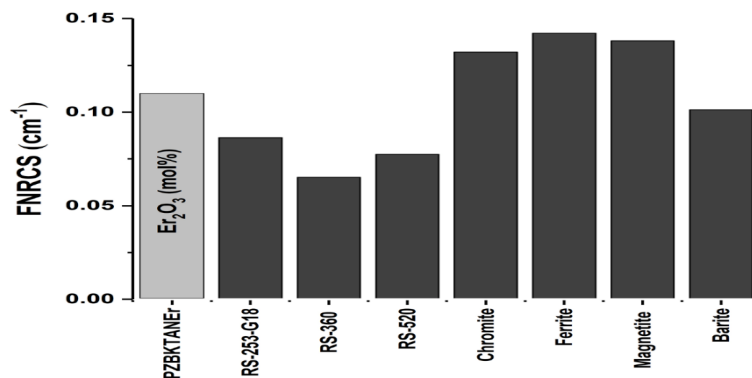


Fig. 8. Histogram illustrating the measured fast neutron-removal cross-sections (FNRCs) for the New protecting material constituents (PZBKTA_{Er} by 3% Er_2O_3) and for other recognized radiation-shielding resources.

Ultimately, we tested the rapid neutron shielding abilities of the projected oxide glass (PZBKTA_{Er} by 3 % Er_2O_3). For the novel glass material and the other shielding materials, the Fast Neutron-removal Cross-Section (FNRCs) values were calculated (Figure- 8). PZBKTA_{Er} with a 3% Er_2O_3 composition showed equivalent FNRCs values to other commercially available shielding products. This means that PZBKTA_{Er}'s neutron shielding performance with a 3% Er_2O_3 composition is slightly increased. The novel glass material showed less hardening efficiency for neutrons when was compared with the marketable radiation protecting glasses like RS-253 G18, RS-360, and RS-520. For example, the documented Fast Neutron-removal Cross-Section measurements showed a recorded percentage variance of ~ 23.03 % for PZBKTA_{Er} with 3% Er_2O_3 , and RS-253-G18 glass. The registered Fast Neutron-removal Cross-Section values showed a recorded percentage variance of ~ 51.13 % with PZBKTA_{Er} with 3% Er_2O_3 and RS-360 glass.

Figure 9 depicts the usual Raman spectra of phosphate glass. The phosphate glasses' structure is mostly constituted of Q_p^n of PO₄ tetrahedra where; n = number of bridging oxygen per PO₄ tetrahedron. The symmetric stretching of P-O is assigned at 1300 cm⁻¹ of an asymmetric profile, the symmetric stretching of a nonbridging oxygen on a Q_p^n tetrahedron is assigned at 1200 cm⁻¹, P-O-P symmetric vibrations are assigned at 700 cm⁻¹, and the symmetric stretching of the orthophosphate groups is assigned near 950 cm⁻¹. Cross-linking between short P-O structural units is provided by P-O-Al connections.

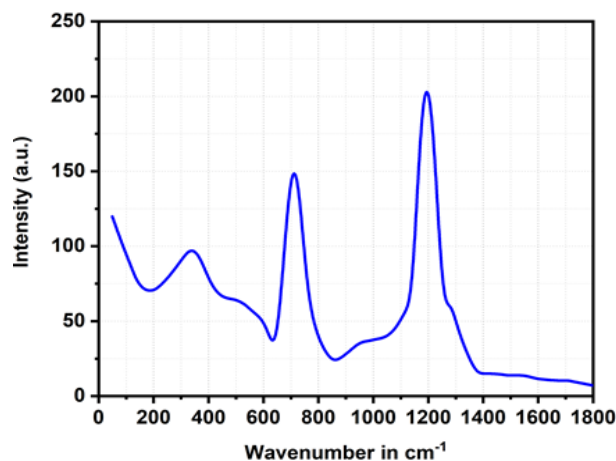


Fig. 9. Raman spectra of fabricated glass (PZBKTAner by 3% Er₂O₃).

4. Conclusion

Ionizing radiation with a wide range of energy and frequencies is leading to a new technological revolution in many fields of science and medicine. However, strict and reliable radiation safety procedures and guidelines need to be put in place to allow the effective use of these technologies. Radiation protection products are a key component of these technologies and procedures. In this study, we analyzed a new oxide glass (PZBKTAner) with Phy-X / PSD software for ionizing radiation ranging from 0.015 to 15 MeV. The results of the modeling process showed a relationship between the energy of the incoming photon and the values observed by the linear attenuation coefficient (LAC) and the mass attenuation coefficient (MAC) and our novel glass performed better than other glasses being used for radiation protection commercially.

Moreover, our Novel Glass material has slightly lower Half-value layer (HVL) measurements than radiation protection materials of healthcare units and other protective equipment's. In addition, PZBKTAner showed significantly better measured Atomic Cross-section (ACS) and the Electronic Cross-section (ECS) values than the other supplies mainly used for radiation protection in different industries and health services. A similar trend is seen for effective atomic and electron numbers (Z_{eff} and N_{eff}) measurements for PZBKTAner, higher values were reported for studied material than the radiation shielding materials used mainly in the medical and technical fields. This study shows that the newly formed glass material can be used for several radiation shielding purposes in both medical and technical sites.

Acknowledgments

This work was supported by the Deanship of Scientific Research at Najran University for funding this work under the Research Collaboration Funding program grant code (NU/RC/MRC/11/3). Also, the authors are thankful the King Khalid University, through a grant

(RCAMS/KKU/04-22) under the Research Center for Advanced Material Science (RCAMS) at King Khalid University, Saudi Arabia.

References

- [1] Singh J, Singh H, Sharma J, Singh T, Singh PS. Fusible alloys: A potential candidate for gamma rays shield design. *Progress in Nuclear Energy*. 2018 Jul 1; 106:387-95; <https://doi.org/10.1016/j.pnucene.2018.04.002>
- [2] Parker HMOD, Joyce MJ, *Progress in Nuclear Energy*. 2015; 85:297-318; <https://doi.org/10.1016/j.pnucene.2015.06.006>
- [3] Vreysen MJB, Robinson AS. Ionising Radiation and Area-Wide Management of Insect Pests to Promote Sustainable Agriculture. 2011:671-92; https://doi.org/10.1007/978-94-007-0394-0_29
- [4] A. Azuraida, M. K. Halimah, M. Ishak, N. R. Fadhilah, A. Norhayati, N. Ahmad. *Chalcogenide Letters*, 18(3), 123 (2021).
- [5] A. Azuraida, M. K. Halimah, M. Ishak, L. Hasnimulyai, S. I. Ahmad, *Chalcogenide Letters*, 17(4), 187 (2020).
- [6] Vano E. Global view on radiation protection in medicine. *Radiat Prot Dosimetry*. 2011;147(1-2):3-7; <https://doi.org/10.1093/rpd/ncr265>
- [7] Mettler FA. Medical effects and risks of exposure to ionising radiation. *Journal of Radiological Protection*. 2012;32(1): N9-N13; <https://doi.org/10.1088/0952-4746/32/1/N9>
- [8] Holmberg O, Malone J, Rehani M, McLean D, Czarwinski R., *European Journal of Radiology*. 2010;76(1):15-9; <https://doi.org/10.1016/j.ejrad.2010.06.033>
- [9] Magrini SM, Pasinetti N, Belgioia L, Triggiani L, Levis M, Ricardi U, et al., *Radiol Med*. 2019;124(8):777-82; <https://doi.org/10.1007/s11547-019-01043-7>
- [10] Jakubowska T, Długosz-Lisiecka M., *Radiation Physics and Chemistry*. 2020; 171:108688; <https://doi.org/10.1016/j.radphyschem.2020.108688>
- [11] Singh VP, Badiger NM, Kaewkhao J., *Journal of Non-Crystalline Solids*. 2014; 404:167-73; <https://doi.org/10.1016/j.jnoncrysol.2014.08.003>
- [12] Singh K, Singh S, Dhaliwal AS, Singh G., *Appl Radiat Isot*. 2015; 95:174-9; <https://doi.org/10.1016/j.apradiso.2014.10.022>
- [13] Schueler BA., *Techniques in Vascular and Interventional Radiology*. 2010;13(3):167-71; <https://doi.org/10.1053/j.tvir.2010.03.005>
- [14] Li Q, Wei Q, Zheng W, Zheng Y, Okosi N, Wang Z, et al., *ACS Appl Mater Interfaces*. 2018;10(41):35510-5; <https://doi.org/10.1021/acsami.8b10600>
- [15] Nagaraja N, Manjunatha HC, Seenappa L, Sridhar KN, Ramalingam HB., *Radiation Physics and Chemistry*. 2020; 171:108723; <https://doi.org/10.1016/j.radphyschem.2020.108723>
- [16] Akman F, Khattari ZY, Kaçal MR, Sayyed MI, Afaneh F., *Radiation Physics and Chemistry*. 2019; 160:9-14; <https://doi.org/10.1016/j.radphyschem.2019.03.001>
- [17] Tijani SA, Kamal SM, Al-Hadeethi Y, Arib M, Hussein MA, Wageh S. et al., *Journal of Alloys and Compounds*. 2018; 741:293-9; <https://doi.org/10.1016/j.jallcom.2018.01.109>
- [18] Waly E-SA, Al-Qous GS, Bourham MA., *Radiation Physics and Chemistry*. 2018; 150:120-4; <https://doi.org/10.1016/j.radphyschem.2018.04.029>
- [19] Al-Assiri MS, Algarni H, Reben M, Yousef E, Hegazy HH, AbouDeif YM, Umar Ahmad, *Optical Materials* 2017; 73: 284-9; <https://doi.org/10.1016/j.optmat.2017.08.030>
- [20] Singh VP, Badiger NM, Chanthima N, Kaewkhao J. Evaluation of gamma-ray exposure buildup factors and neutron shielding for bismuth borosilicate glasses. *Radiation Physics and Chemistry*. 2014 May 1; 98:14-21; <https://doi.org/10.1016/j.radphyschem.2013.12.029>
- [21] Ersundu AE, Büyükyıldız M, Çelikbilek Ersundu M, Şakar E, Kurudirek M. The heavy metal oxide glasses within the WO₃-MoO₃-TeO₂ system to investigate the shielding properties of radiation applications. *Progress in Nuclear Energy*. 2018 Apr 1; 104:280-7; <https://doi.org/10.1016/j.pnucene.2017.10.008>

- [22] El-Khayatt AM, Ali AM, Singh VP. Photon attenuation coefficients of Heavy-Metal Oxide glasses by MCNP code, XCOM program and experimental data: A comparative study. *Nuclear Instruments and Methods in Physics Research, Section A: Accelerators, Spectrometers, Detectors and Associated Equipment.*;735:207-12; <https://doi.org/10.1016/j.nima.2013.09.027>
- [23] Dong MG, Agar O, Tekin HO, Kilicoglu O, Kaky KM, Sayyed MI. A comparative study on gamma photon shielding features of various germinate glass systems. *Composites Part B.* 2019 Jan 1 ;165: 636-647; <https://doi.org/10.1016/j.compositesb.2019.02.022>
- [24] Waly E-SA, Fusco MA, Bourham MA., *Annals of Nuclear Energy.* 2016; 96:26-30; <https://doi.org/10.1016/j.anucene.2016.05.028>
- [25] Lakshminarayana G, Baki SO, Kaky KM, Sayyed MI, Tekin HO, Lira A, et al., *Journal of Non-Crystalline Solids.* 2017; 471:222-37; <https://doi.org/10.1016/j.jnoncrysol.2017.06.001>
- [26] Shamshad L, Rooh G, Limkitjaroenporn P, Srisittipokakun N, Chaiphaksa W, Kim HJ, et al., *Progress in Nuclear Energy.* 2017; 97:53-9; <https://doi.org/10.1016/j.pnucene.2016.12.014>
- [27] Chanthima N, Kaewkhao J, Limkitjaroenporn P, Tuscharoen S, Kothan S, Tungjai M, et al., *Radiation Physics and Chemistry.* 2017; 137:72-7; <https://doi.org/10.1016/j.radphyschem.2016.03.015>
- [28] Lakshminarayana G, Elmahroug Y, Kumar A, Dong MG, Lee D-E, Yoon J, et al. Li₂O-B₂O₃-Bi₂O₃ glasses: gamma-rays and neutrons attenuation study using ParShield/WinXCOM program and Geant4 and Penelope codes. *Applied Physics A.* 2020;126(4); <https://doi.org/10.1007/s00339-020-3418-7>
- [29] Şakar E, Özpolat ÖF, Alım B, Sayyed MI, Kurudirek M., *Radiation Physics and Chemistry.* 2020; 166:108496-12; <https://doi.org/10.1016/j.radphyschem.2019.108496>
- [30] Tijani SA, Kamal SM, Al-Hadeethi Y, Arib M, Hussein MA, Wageh S, et al., *Journal of Alloys and Compounds.* 2018; 741:293-9; <https://doi.org/10.1016/j.jallcom.2018.01.109>
- [31] Qi F, Huang F, Wang T, Ye R, Lei R, Tian Y, et al., *Journal of Luminescence.* 2018; 202:132-5; <https://doi.org/10.1016/j.jlumin.2018.05.049>
- [32] Şakar E, Özpolat ÖF, Alım B, Sayyed MI, Kurudirek M., *Radiation Physics and Chemistry.* 2020; 166:108496-12; <https://doi.org/10.1016/j.radphyschem.2019.108496>
- [33] Mahmoud KA, Sayyed MI, Tashlykov OL., *Nuclear Engineering and Technology.* 2019;51(7):1835-41; <https://doi.org/10.1016/j.net.2019.05.013>
- [34] Chilton AB, Shultis JK, Faw RE. *Principles of Radiation Shielding.* 1st ed. New Jersey: Prentice Hall; 1984; https://doi.org/10.1007/978-1-4939-2493-6_25-5
- [35] Gerward L, Guilbert N, Jensen KB, Leving H. WinXCom-a program for calculating X-ray attenuation coefficients. *Radiation Physics and Chemistry.* 2004;71(3-4):653-4; <https://doi.org/10.1016/j.radphyschem.2004.04.040>
- [36] Sayyed MI., *Journal of Alloys and Compounds.* 2017; 695:3191-7; <https://doi.org/10.1016/j.jallcom.2016.11.318>
- [37] Wagh A, Sayyed MI, Askin A, Özpolat ÖF, Sakar E, Lakshminarayana G, et al., *Solid State Sciences.* 2019; 96:105959; <https://doi.org/10.1016/j.solidstatesciences.2019.105959>
- [38] Sayyed MI, Çelikkbilek Ersundu M, Ersundu AE, Lakshminarayana G, Kostka P., *Radiation Physics and Chemistry.* 2018; 144:419-25; <https://doi.org/10.1016/j.radphyschem.2017.10.005>
- [39] Alım B. Determination of Radiation Protection Features of the Ag₂O Doped Boro-Tellurite Glasses Using Phy-X / PSD Software. *Journal of the Institute of Science and Technology.*2020:202-13; <https://doi.org/10.21597/jist.640027>
- [40] Harima Y, Kurosawa N, Sakamoto Y., *Progress in Nuclear Science and Technology.* 2014; 4:548-52; <https://doi.org/10.15669/pnst.4.548>
- [41] Sharaf JM, Saleh H., *Radiation Physics and Chemistry.* 2015; 110:87-95; <https://doi.org/10.1016/j.radphyschem.2015.01.031>
- [42] Singh VP, Badiger NM., *Journal of Ceramics.* 2013; 2013:1-13; <https://doi.org/10.1155/2013/967264>